IAC-22-C1.9.4

Semi-analytical estimation of the probability of capture into ground-track resonances of Dawn around Vesta.

Wail Boumchita[1, a], **Jinglang Feng**[1, b], **Anatoly Neishtadt**[2, c]

[1] *Department of Mechanical and Aerospace Engineering (Aerospace Center of Excellence), University of Strathclyde, 75 Montrose Street, Glasgow G1 1XJ, United Kingdom.*
[2] *Loughborough University, LE11 3TU Loughborough, United Kingdom*
[a] *wail.boumchita@strath.ac.uk*
[b] *jinglang.feng@strath.ac.uk*
[c] *a.neishtadt@lboro.ac.uk*

Abstract

This paper presents a semi-analytical methodology to estimate the probability of capture into different ground-track resonances of a low-thrust spacecraft around an asteroid. The system dynamics are described by a Hamiltonian model that considers the perturbations from the irregular gravitational field up to the second order and degree, and the continuous low thrust that remains constant in magnitude and is always in the direction opposite to the spacecraft's velocity. The model focuses on the equatorial case of the 1:1 and 2:3 ground-track resonances. Due to the chaotic layer around each resonance region, which influences the orbit evolution, estimating the probability of capture into resonance is necessary. A fourth-order polynomial is used to numerically approximate the separatrices of the resonance region, while the change of the system's energy balance when the trajectory crosses the separatrices is determined with a global adaptive quadrature method. Subsequently, the probability of capture into resonance is estimated from the energy change as the trajectory crosses the separatrices, and the accuracy of the results is verified by comparing them to numerical simulations based on the perturbed Hamilton's equations of motion. This research makes a significant contribution to the field of astrodynamics by systematically and efficiently analyzing the probability of low-thrust spacecraft capture into different ground-track resonance around asteroids.

Keywords: Semi-analytical methods, Resonance capture, Astrodynamics, Vesta, Gravitational perturbations, Low-thrust propulsion

1 Introduction

Resonance is a pervasive phenomenon in dynamical systems, arising when a system is excited at its natural frequency, thereby causing pronounced oscillations. This concept manifests across diverse disciplines, including plasma physics [1], celestial mechanics [2], and astrodynamics [3]. Within the realms of celestial mechanics and astrodynamics, various forms of orbital resonances are evident. These range from mean motion resonances, where the orbital periods of two celestial bodies are in simple integer ratios [4], to more complex forms like secular [5], secondary [6], spin-orbit [7], and ground-track resonances (GTRs) [3]. Notably, for GTRs to manifest, the period of a spacecraft's revolution must be commensurable with the rotation period of the central body, as exemplified in 1:1 GTRs with Earth's geostationary satellites [8]. Previous studies have delved into the impact of irregular gravitational fields on resonant satellite orbits. Scheeres [9] focused on satellites orbiting irregularly shaped asteroids, particularly investigating periodic orbits around the ellipsoids mimicking asteroids Vesta and Eros. Subsequent extensions of this work explored the asteroid Toutatis [10] and the moons Europa [11] [12] [13] and Enceladus [14] [15].

This paper focuses on the Dawn mission around the asteroid Vesta. In 2011, the Dawn spacecraft successfully arrived at the asteroid Vesta. During the approach phase, the spacecraft descended from a high-altitude mission orbit (HAMO) to a low-altitude mission orbit (LAMO) utilizing low-thrust propulsion. The orbital radii of the HAMO and LAMO are 1000 km and 460 km, respectively [3]. However, the use of low-thrust propulsion during the descent phase posed a risk of capturing the spacecraft into GTR around Vesta, caused by the chaotic layer surrounding the resonance region [8]. This mission demonstrated the possibility of relying on low-thrust propulsion for the

majority of the mission duration [16] [17]. The use of low-thrust propulsion allows for more efficient use of fuel and longer mission duration but also poses some challenges in terms of trajectory design [18]. However, the motion around Vesta is more complex due to its irregular gravitational field. The spacecraft at each revolution encounters the same gravitational configuration, the effect of which accumulates and significantly changes the orbit eccentricity and inclination [19]. The capture of a spacecraft into a GTR has the potential to significantly impact the success of a mission by preventing the reach of lower altitudes and the achievement of scientific objectives.

The primary aim of this paper is to use the Hamiltonian formalism to analyze the capture into GTR phenomenon and, specifically, estimate the probability of capture into 1:1 and 2:3 GTRs through semi-analytical and analytical approaches. The methodologies presented in this paper are based on analyzing the energy change that occurs when the spacecraft enters into resonance with Vesta's rotational motion. A two-degree-of-freedom Hamiltonian model associated with the 1:1 and 2:3 GTRs in the equatorial case is developed. This includes the perturbations from the irregularities of the gravitational field up to the second order, along with continuous low thrust that remains constant in magnitude and is always in the direction opposite to the spacecraft's velocity. Through this process, the equilibrium points, as well as the libration and circulation regions, are identified. A global adaptive quadrature method is used to evaluate the system's energy balance as the trajectory crosses the separatrix. Then, the probability of capture into GTR is estimated as a function of the energy balance, and the accuracy of the results is verified by comparing them with numerical simulations based on the equations of motion derived from the Hamiltonian of each GTR. A significant advantage of a semi-analytical investigation is the ease with which the results can be obtained when the data changes. Our approach is highly adaptable to similar missions, as the numerical values of parameters such as the shape and mass of the asteroid or spacecraft orbit may vary, but the methodology remains the same, and the results can be readily adapted accordingly.

The paper is organized as follows: Section 2 provides a description of the dynamic model for the motion of Dawn around Vesta and derives the equations of motion. The semi-analytical methodology used to estimate the probability of capture into 1:1 and 2:3 GTRs is presented in Section 3. The results of the semi-analytical and analytical estimations and the comparison with numerical estimations are discussed in Section 4, where the errors are also characterized. Finally, Section 5 lists the advantages and contribution of this work and Section 6 summarizes the paper and presents the conclusions.

2 Dynamic model

This section presents the Hamiltonian that describes the motion of a spacecraft around an asteroid with an irregular gravitational field. Specifically, the Hamiltonian is focused on the 1:1 and 2:3 GTRs in the equatorial case and the resulting equations of motion are derived. The impact of non-conservative forces, such as the low-thrust, is also accounted for. To simplify the model, each Hamiltonian is expanded around the location of the respective GTR, resulting in a pendulum-like expression.

2.1 Hamiltonian model

The gravitational potential of a central body can be represented using spherical harmonics [20], where the shape and density variations of an asteroid are expressed using the Stokes coefficients. The potential, denoted as V, is expressed as a series expansion of spherical harmonics up to degree n and order m as

$$V = \frac{\mu}{r} + \sum_{n=2}^{\infty}\sum_{m=0}^{n}\sum_{p=0}^{n}\sum_{q=-\infty}^{\infty}\frac{\mu R_e^n}{a^{n+1}}F_{nmp}(i) G_{npq}(e)S_{nmpq}(\omega, M, \Omega, \theta) \quad (1)$$

where $\mu = 17.5\,\mathrm{km}^2/\mathrm{s}^3$ is the gravitational constant, $R_e = 300$ km is the reference radius, $F_{nmp}(i)$ and $G_{npq}(e)$ are functions of the inclination i and eccentricity e, respectively, a is the semi-major axis, ω is the argument of periapsis, M is the mean anomaly, Ω is the longitude of the ascending node, θ is the sidereal time and n, m, p, q are all integers and

$$S_{nmpq} = \begin{cases} C_{nm}\cos\Psi_{nmpq} + S_{nm}\sin\Psi_{nmpq} \\ -S_{nm}\cos\Psi_{nmpq} + C_{nm}\sin\Psi_{nmpq} \end{cases} \quad (2)$$

where the first and the second equations are considered if the value of $n-m$ is even or odd respectively and Ψ_{nmpq} is the Kaula's phase angle, defined as

$$\Psi_{nmpq} = (n-2p)\omega + (n-2p+q)M + m(\Omega-\theta). \quad (3)$$

When the rate of change of Kaula's phase angle $\dot{\Psi}_{nmpq}$ is close to zero, the GTRs occur. Let $L = \sqrt{\mu a}$. The

Hamiltonian describing the spacecraft's motion around an asteroid with an irregular gravitational field is defined as

$$\mathcal{H} = -\frac{\mu^2}{2L^2} + \sum_{n=2}^{\infty}\sum_{m=0}^{n}\sum_{p=0}^{n}\sum_{q=-\infty}^{\infty} R_e^n \frac{\mu^{n+2}}{L^{2n+2}} F_{nmp}(i)G_{npq}(e)S_{nmpq}(\omega, M, \Omega, \theta) + \dot{\theta}\Lambda \quad (4)$$

where $\dot{\theta} = 3.2671\times10^{-4}$ rad/s is Vesta's angular velocity, Λ is the conjugate momentum to the sidereal time θ and the term $\dot{\theta}\Lambda$ accounts for the asteroid's rotation.

2.1.1 1:1 GTR

The gravitational term of second degree and order primarily affects the dynamics of the system close to the 1:1 GTR [21]. Therefore, the Hamiltonian used in the analysis considers only this harmonic. The Hamiltonian that describes the 1:1 GTR dynamics around the asteroid is expressed as

$$\mathcal{H}_{1:1} = -\frac{\mu^2}{2L^2} + R_e^2\frac{\mu^4}{L^6}F_{220}(i) G_{200}(e)S_{2200}(\omega, M, \Omega, \theta) + \dot{\theta}\Lambda. \quad (5)$$

For an equatorial orbit ($i = 0°$), the Hamiltonian is

$$\mathcal{H}_{1:1} = -\frac{\mu^2}{2L^2} - \frac{15}{2}R_e^2\frac{\mu^4}{L^6}\left(-\frac{3}{5} + \frac{G^2}{L^2}\right) C_{22}\cos(2(M+\omega-\theta)) + \dot{\theta}\Lambda, \quad (6)$$

where $C_{22} = 3.079667257459264 \times 10^{-3}$ is the second degree and order Stokes coefficient, L and $G = L\sqrt{1-e^2}$ are the momenta conjugate respectively to M and ω. A canonical transformation is performed with the generating function $F_1 = (M+\omega-\theta)L' + (-\omega)G' + \theta\Lambda'$ which leads to the new set of canonical variables

$$\sigma = M + \omega - \vartheta \quad , \quad Q = -\omega \quad , \quad L = L' \quad (7)$$
$$G = L' - K \quad , \quad \Lambda = -L' + \Lambda'. \quad (8)$$

The new Hamiltonian $\tilde{\mathcal{H}}_{1:1}$ is

$$\tilde{\mathcal{H}}_{1:1} = -\frac{\mu^2}{2L^2} - \frac{15}{2}R_e^2\frac{\mu^4}{L^6}\left(-\frac{3}{5} + \frac{(L-K)^2}{L^2}\right) C_{22}\cos(2\sigma) - \dot{\theta}L, \quad (9)$$

where the prime sign and the non-essential term $\dot{\theta}\Lambda'$ are dropped for brevity. Fig. 1 shows the phase portrait of $\tilde{\mathcal{H}}_{1:1}$, where the upper separatrices are indicated with the red line l_1 and the lower ones with l_2.

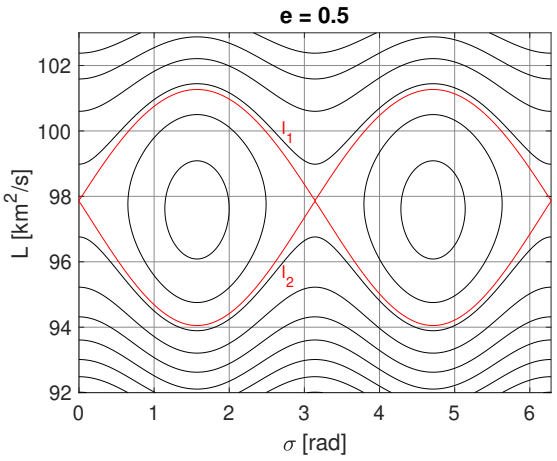

Figure 1: Phase space of the 1:1 GTR for $e = 0.5$. The red lines represent the separatrix lines. The eccentricity value is determined by fixing $L = L_r$ and $K = K_{sep}$ related to the 1:1 GTR.

2.1.2 2:3 GTR

Similarly to the 1:1 GTR, the gravitational term of second degree and order primarily affects the dynamics of the system close to the 2:3 GTR. The Hamiltonian that describes the 2:3 GTR dynamics around the asteroid for an equatorial orbit is expressed as

$$\mathcal{H}_{2:3} = -\frac{\mu^2}{2L^2} - \frac{21}{2}\sqrt{1-\left(\frac{G}{L}\right)^2}R_e^2\frac{\mu^4}{L^6} C_{22}\cos[3(M+\omega) - 2\theta - \omega] + \dot{\theta}\Lambda \quad (10)$$

A canonical transformation is performed with the generating function $F_2 = [3(M+\omega) - 2\theta]L' + (-\omega)G' + \theta\Lambda'$ which leads to the new set of canonical variables

$$\sigma = 3M + 3\omega - 2\theta \quad , \quad g = -\omega \quad , \quad L = 3L'$$
$$G = 3L' - G' \quad , \quad \Lambda = -2L' + \Lambda'$$

The new Hamiltonian $\hat{\mathcal{H}}_{2:3}$ is

$$\hat{\mathcal{H}}_{2:3} = -\frac{\mu^2}{18L'^2} - \frac{21}{2}\sqrt{1-\left(\frac{3L'-G'}{3L'}\right)^2} R_e^2\frac{\mu^4}{(3L')^6}C_{22}\cos(\sigma+g) - 2\dot{\theta}L' \quad (11)$$

where the non-essential term $\dot{\theta}\Lambda'$ is dropped. A second canonical transformation is performed with the generating function $F_2' = (\sigma+g)L'' + kK + \theta\Lambda''$ which leads to the new set of canonical variables

$$\sigma' = \sigma + g \quad , \quad L' = L'' \quad , \quad G' = L'' + K$$

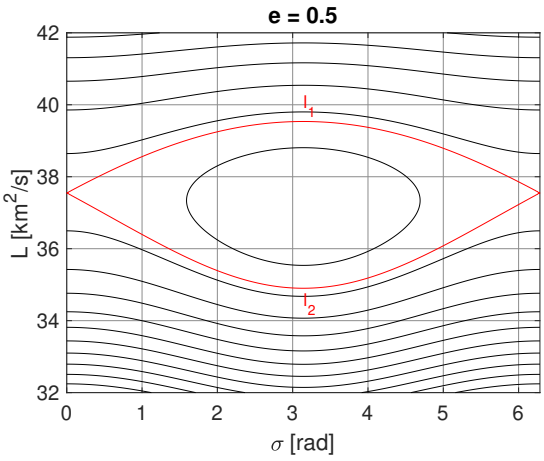

Figure 2: Phase space of the 2:3 GTR for $e = 0.5$. The red lines represent the separatrix lines. The eccentricity value is determined by fixing $L = L_r$ and $K = K_{sep}$ related to the 2:3 GTR.

The new Hamiltonian $\tilde{\mathcal{H}}_{2:3}$ is

$$\tilde{\mathcal{H}}_{2:3} = -\frac{\mu^2}{18L^2} - \frac{21}{2}\sqrt{1-\left(\frac{2L-K}{3L}\right)^2} R_e^2 \frac{\mu^4}{(3L)^6} C_{22}\cos(\sigma) - 2\dot{\theta}L \quad (12)$$

where the prime and double prime signs have been dropped. Fig. 2 shows the phase portrait of $\tilde{\mathcal{H}}_{2:3}$, where the upper separatrix is indicated with the red line l_1 and the lower one with l_2.

2.2 Pendulum approximation

In this section, an approximation of the complete Hamiltonian model of the 1:1 and 2:3 GTRs is presented.

2.2.1 1:1 GTR

Considering Eq. 9, the Hamiltonian is defined as

$$\tilde{\mathcal{H}}_{1:1} = -\frac{\mu^2}{2L^2} - A(L,K)\cos(2\sigma) - \dot{\theta}L \quad (13)$$

The 1:1 GTR is located at $L = L_r$ defined from

$$\frac{\mu^2}{L_r^3} = \dot{\theta} \quad (14)$$

Then, the Hamiltonian is expanded around the resonance up to the second order leading to

$$\hat{\mathcal{H}}_{1:1} = -\frac{1}{2}\alpha p^2 - \hat{A}(L_r,K)\cos(2\sigma), \quad (15)$$

where

$$\hat{A}(L_r,K) = \frac{15}{2}R_e^2\frac{\mu^4}{L_r^6}\left(-\frac{3}{5}+\frac{(L_r-K)^2}{L_r^2}\right)C_{22} \quad (16)$$

$$\alpha = \frac{3\mu^2}{L_r^4} \quad (17)$$

and the constant term is discarded. The Hamiltonian $\hat{\mathcal{H}}_{1:1}$ resembles the structure of a pendulum's Hamiltonian, composed of two main components: a quadratic term that represents the system's kinetic energy, and another term that accounts for the system's potential energy.

2.2.2 2:3 GTR

From Eq. 12, the Hamiltonian $\tilde{\mathcal{H}}_{2:3}$ is

$$\tilde{\mathcal{H}}_{2:3} = -\frac{\mu^2}{18L^2} - \frac{21}{2}\sqrt{1-\left(\frac{2L-K}{3L}\right)^2} R_e^2\frac{\mu^4}{(3L)^6}C_{22}\cos(\sigma) - 2\dot{\theta}L \quad (18)$$

The 2:3 GTR is located at $L = L_r$ defined from

$$\frac{\mu^2}{18L_r^3} = \dot{\theta} \quad (19)$$

The Hamiltonian $\tilde{\mathcal{H}}_{2:3}$ is expanded around the resonance as

$$\hat{\mathcal{H}}_{2:3} = -\frac{1}{2}\alpha p^2 - \hat{A}(L_r,K)\cos(\sigma) \quad (20)$$

where

$$\hat{A}(L_r,K) = \frac{21}{2}\sqrt{1-\left(\frac{2L_r-K}{3L_r}\right)^2} R_e^2\frac{\mu^4}{(3L_r)^6}C_{22} \quad (21)$$

$$\alpha = \frac{\mu^2}{3L_r^4} \quad (22)$$

and the constant term is discarded. As for the 1:1 GTR, the Hamiltonian $\hat{\mathcal{H}}_{2:3}$ resembles the structure of a pendulum's Hamiltonian.

2.3 Dissipative Forces into Hamiltonian Formalism

One approach to account for energy dissipation in Hamiltonian mechanics is to introduce a term in the perturbed Hamilton's equations of motion that accounts for the presence of dissipative forces [22].

2.3.1 1:1 GTR

The change of L over time can be related to the change of a as

$$\frac{dL}{dt} = \frac{\mu}{2L}\frac{da}{dt}. \tag{23}$$

From [23], the rate of change of the semi latus rectum $p = a(1-e^2)$ due to tangential accelerations is

$$\frac{dp}{dt} = \frac{2}{v}a_t p, \tag{24}$$

where v is the spacecraft velocity and a_t is the magnitude of the tangential acceleration from the low-thrust. So,

$$\frac{dL}{dt} = T_L = -\frac{T}{m}\frac{L^2}{\mu}. \tag{25}$$

Since $K = L - G$, the rate of change of K over time is

$$\frac{dK}{dt} = \frac{dL}{dt} - \frac{dG}{dt}. \tag{26}$$

The rate of change of G over time is related to the rate of change of e as

$$\frac{dG}{dt} = -\frac{T}{m}\frac{LG}{\mu} - e\frac{L^2}{G}\frac{de}{dt}. \tag{27}$$

From [23], the rate of change of e due to the low-thrust is

$$\frac{de}{dt} = \frac{1}{v}\left(-2\frac{T}{m}(e+\cos\theta)\right). \tag{28}$$

To eliminate the dependency on the true anomaly, the expression is averaged over the mean anomaly. Considering the second term of de/dt, the following integral is defined

$$I = \frac{1}{2\pi}\int_0^{2\pi}\cos\theta dM. \tag{29}$$

The integrand and the differential of the mean anomaly are expressed as functions of the eccentric anomaly E as

$$\cos\theta = \frac{\cos E - e}{1 - e\cos E} \quad \text{and} \quad dM = (1 - e\cos E)dE. \tag{30}$$

So the integral I becomes

$$I = \frac{1}{2\pi}\int_0^{2\pi}(\cos E - e)dE = -e. \tag{31}$$

Therefore, $de/dt = 0$. Finally, the rate of change of K is

$$\frac{dK}{dt} = T_K = -\frac{T}{m}\frac{LK}{\mu}. \tag{32}$$

Introducing the variable $p = L - Lr$, the perturbed Hamilton's equations of motion are

$$\begin{cases} \dot{\sigma} = \frac{d\tilde{\mathcal{H}}_{1:1}}{dp} \\ \dot{p} = -\frac{d\tilde{\mathcal{H}}_{1:1}}{d\sigma} + T_L \\ \dot{K} = T_K \end{cases} \tag{33}$$

Fig. 3 shows the numerical verification of the resonance capture phenomenon for $e = 0.5$, with a set of uniformly distributed initial resonance angles between [0,2π] and the initial altitude of 700 km.

The simulation results indicate that the spacecraft is captured into resonance, as highlighted in red in Fig. 3. Once captured, the momentum p exhibits libration around the resonance location at $p = 0$, as shown in the upper left plot of Fig. 3. The upper right plot in Fig. 3 shows the trajectory of the system in phase space, where the trajectory captured into resonance rotates around the stable equilibrium point (σ,p) = (π/2,0). During the system's evolution, the momentum K decreases, and e remains almost constant until the separatrix crossing. After that, e starts to oscillate, and the average value decreases over time.

2.3.2 2:3 GTR

From Eqs. 25 and 32 and applying the previous canonical transformations, the effect of low-thrust on L and G is

$$T_L = -\frac{T}{m}\frac{L^2}{\mu} \tag{34}$$

$$T_G = -\frac{T}{m}\frac{L}{\mu}LG \tag{35}$$

Since $L' = 1/3L$ and $G' = 3L' - G$, we have

$$T_{L'} = \frac{1}{3}T_L = -\frac{1}{3}\frac{T}{m}\frac{L'^2}{\mu} \tag{36}$$

$$T_{G'} = T_L - T_G = -\frac{T}{m}\frac{L'^2 - L'G'}{\mu} \tag{37}$$

Next, as $L'' = L'$ and $K = G' - L'$, we have

$$T_{L''} = T_{L'} = -\frac{1}{3}\frac{T}{m}\frac{L''^2}{\mu} \tag{38}$$

$$T_K = T_{G'} - T_{L'} = -\frac{2}{3}\frac{T}{m}\frac{L'^2}{\mu} + \frac{T}{m}\frac{L'G'}{\mu} \tag{39}$$

Finally, substituting the expression of the new variables into Eqs.38 and 39,the rate of change of the conjugate momenta due to low-thrust is defined as

$$T_L = -3\frac{T}{m}\frac{L^2}{\mu} \tag{40}$$

$$T_K = -3\frac{T}{m}\frac{LK}{\mu} \tag{41}$$

where the prime and double prime signs have been dropped. So, the perturbed Hamilton's equations of motion are

$$\begin{cases} \dot{\sigma} = \frac{d\tilde{\mathcal{H}}_{2:3}}{dp} \\ \dot{p} = -\frac{d\tilde{\mathcal{H}}_{2:3}}{d\sigma} + T_L \\ \dot{K} = T_K \end{cases} \tag{42}$$

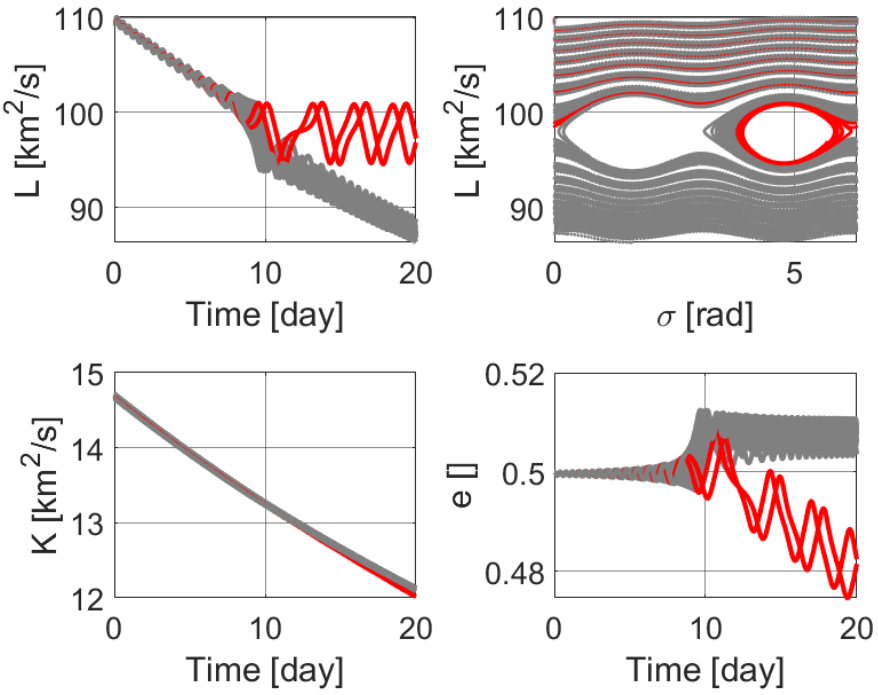

Figure 3: Trajectory evolution over time in the case of crossing the 1:1 GTR. The capture cases are highlighted in red. The upper plots show the evolution of L over time and in phase space, respectively. The lower left and right plots show the evolution of K and of the eccentricity over time, respectively.

where $p = L - L_r$, the resonance capture is numerically verified for fixed values of $e = 0.5$ as shown in Fig. 4. The simulations are performed considering a uniformly distributed set of initial resonance angles, and the initial altitude considered is 1000 km, as the location of the 2:3 resonance is at 720 km.

3 Methodology

This section presents the semi-analytical methodology to estimate the probability of capture into 1:1 GTR. The domain (σ,p) where the initial conditions are uniformly distributed is defined and denoted by U. A subset of initial conditions, labeled as U_{res}, can be identified within this domain, which corresponds to the capture of the system into the resonance domain. Then, the probability of capture into resonance can be determined by

$$Pr = \frac{\text{mes}U_{res}}{\text{mes}U}, \tag{43}$$

where mesU_{res} and mes$U$ are the volumes of domains of U_{res} and U in phase space, respectively. This formulation is suitable only for numerical evaluation of the probability. To obtain an analytical estimation, it is necessary to express the probability in a different form using the energy-related quantities of the system.

3.1 1:1 GTR

From [24], the probability of capture into 1:1 GTR is defined as

$$Pr = \frac{\int_{l_1 \cup l_2} d\tilde{\tilde{\mathcal{H}}}_{1:1}/dt\, d\tau}{\int_{l_1} d\tilde{\tilde{\mathcal{H}}}_{1:1}/dt\, d\tau}, \tag{44}$$

where $\tilde{\tilde{\mathcal{H}}}_{1:1} = \tilde{\mathcal{H}}_{1:1} - \tilde{\mathcal{H}}_{SP}$ and $\tilde{\mathcal{H}}_{SP}$ is the value of the Hamiltonian $\tilde{\mathcal{H}}_{1:1}$ at the saddle point. The integral in the numerator is computed along the upper separatrix l_1 and the lower separatrix l_2, whereas the integral in the denominator is calculated only along the upper separatrix. These integrals are improper as the motion along a separatrix takes an infinite amount of time. Thus, the normalization of the Hamiltonian guarantees the convergence of the integrals [25].

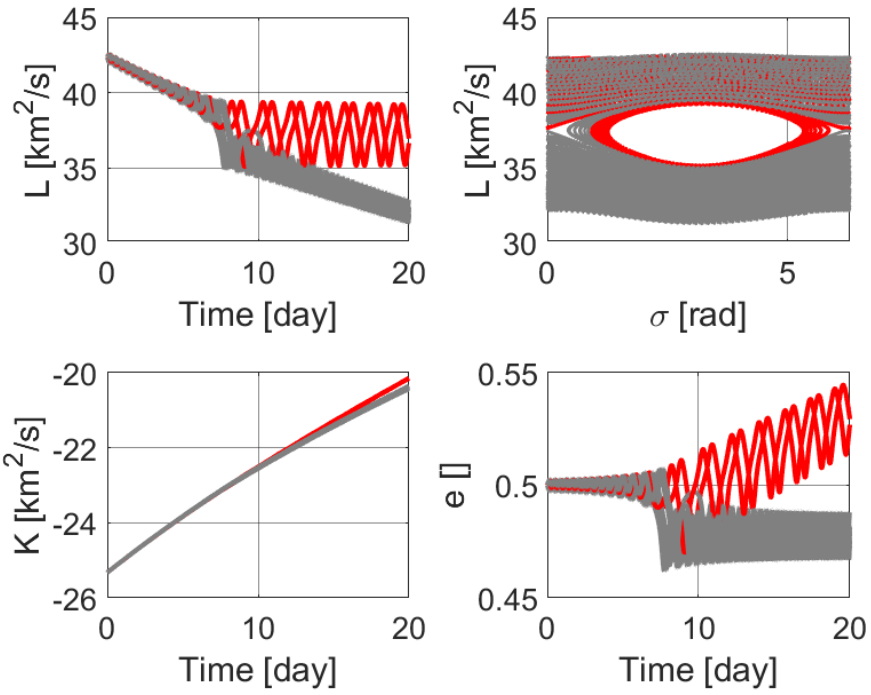

Figure 4: Trajectory evolution over time in the case of crossing the 2:3 GTR. The capture cases are highlighted in red. The upper plots show the evolution of L over time and in phase space, respectively. The lower left and right plots show the evolution of K and of the eccentricity over time, respectively.

3.1.1 Complete model

The probability estimation is based on the normalized complete Hamiltonian model $\tilde{\tilde{\mathcal{H}}}_{1:1}$. The saddle points are defined from

$$\frac{\partial \tilde{\tilde{\mathcal{H}}}_{1:1}}{\partial p} = 0. \tag{45}$$

Next, the values of the separatrices p_{sep} are determined numerically using an N-th polynomial function. Specifically, this involves fixing the value of $K = K_{sep}$ at the point when the system crosses the separatrix

$$p_{sep} = \sum_{i=0}^{N} c_i \sigma^i. \tag{46}$$

It is found that the separatrices are approximated with good accuracy with a 4th order polynomial. The lower and upper separatrices are identified as p_{sep}^{low} and p_{sep}^{up}. Firstly, the integral at the denominator of Eq. 44 is solved as

$$\int_{l_1} \frac{d\tilde{\tilde{\mathcal{H}}}_{1:1}}{dt} d\tau = \int_{l_1} \frac{\partial \tilde{\tilde{\mathcal{H}}}_{1:1}}{\partial p} T_L d\tau + \int_{l_1} \frac{\partial \tilde{\tilde{\mathcal{H}}}_{1:1}}{\partial K} T_K d\tau = \tag{47}$$

$$= \int_{\pi}^{0} T_L d\sigma + \int_{\pi}^{0} \frac{\partial \tilde{\tilde{\mathcal{H}}}_{1:1}}{\partial K} \frac{1}{\partial \tilde{\tilde{\mathcal{H}}}_{1:1}/\partial p} T_K d\sigma. \tag{48}$$

The expression is evaluated at $p = p_{sep}^{up}(\sigma)$ and numerically integrated using the global adaptive quadrature method [26]. The global adaptive quadrature divides the integration domain into smaller subintervals and compute the integral over each subinterval separately. The integral is then approximated as the sum of the integrals over the subintervals. The subintervals are chosen in such a way that the error in the approximation is minimized. In a similar way, the numerator is developed as

$$\int_{l_1 \cup l_2} \frac{d\mathcal{H}_{1:1}}{dt} d\tau = \int_{l_1} \frac{d\mathcal{H}_{1:1}}{dt} d\tau + \int_{l_2} \frac{d\mathcal{H}_{1:1}}{dt} d\tau \tag{49}$$

The first term is identical to the one already developed, while the second term is developed in a similar way

$$\int_{l_2} \frac{d\mathcal{H}_{1:1}}{dt} d\tau = \int_0^{\pi} T_L d\sigma + \int_0^{\pi} \frac{\partial \mathcal{H}_{1:1}}{\partial K} \frac{1}{\partial \mathcal{H}_{1:1}/\partial p} T_K d\sigma \tag{50}$$

but evaluated at $p = p_{sep}^{low}(\sigma)$.

3.1.2 Pendulum approximation

As for the complete model, the value of the Hamiltonian is normalized, so that $\hat{\bar{\mathcal{H}}}_{1:1} = \hat{\mathcal{H}}_{1:1} - \hat{A}$. The new Hamiltonian $\hat{\bar{\mathcal{H}}}_{1:1}$ is

$$\hat{\bar{\mathcal{H}}}_{1:1} = -\frac{1}{2}\alpha p^2 + 2\hat{A}\sin^2\sigma. \tag{51}$$

The non-conservative contributions T_L and T_K from Eq. 25 and Eq. 32 are approximated as

$$T_L = \varepsilon L^2 \sim \varepsilon(L_r^2 + 2L_r p) \tag{52}$$

$$T_K = \varepsilon LK = \varepsilon(L_r K + Kp), \tag{53}$$

in which the second-order term is neglected. Using the chain rule and Hamilton's equation, the rate of change of $\hat{\bar{\mathcal{H}}}_{1:1}$ is defined as

$$\frac{d\hat{\bar{\mathcal{H}}}_{1:1}}{dt} = -\alpha p T_L + 4\hat{A}\sin\sigma\cos\sigma\, T_\sigma + 2\frac{dA}{dK}\sin^2\sigma\, T_K. \tag{54}$$

Along the separatrix l_1, the Hamiltonian $\hat{\bar{\mathcal{H}}}_{1:1} = 0$, so

$$p_{sep} = \pm 2\sqrt{\frac{A}{\alpha}}\sin\sigma. \tag{55}$$

Combining Eq. 54 and Eq. 55, the probability of capture into 1:1 GTR is

$$Pr = \frac{16L_r\sqrt{\frac{\hat{A}}{\alpha}} - 4\frac{\partial\hat{A}}{\partial K}L_r K\frac{1}{\sqrt{\hat{A}\alpha}}}{\pi L_r^2 + 8L_r\sqrt{\frac{\hat{A}}{\alpha}} - 2L_r K\frac{\partial\hat{A}}{\partial K}\frac{1}{\sqrt{\hat{A}\alpha}} - \frac{\pi}{\alpha}K\frac{\partial\hat{A}}{\partial K}}. \tag{56}$$

The probability formulation is independent of the spacecraft mass and the thrust magnitude, as can be observed from the equation. By analyzing each term, the dominant terms in the probability formulation are identified. For the pendulum approximation, the probability of capture into the 1:1 GTR in the equatorial case is simplified to

$$Pr = \frac{2}{\frac{\pi}{8}\sqrt[3]{\frac{\mu}{\dot{\theta}^2 C_{22}^{3/2} R_e^3}} + 1}. \tag{57}$$

3.2 2:3 GTR

Differently, from the 1:1 GTR case, the numerical integration shall be performed in the interval $[0, 2\pi]$. So

$$\int_{l_1} \frac{d\tilde{\mathcal{H}}_{2:3}}{dt} d\tau = \int_{2\pi}^{0} T_L d\sigma + \int_{2\pi}^{0} \frac{\partial \tilde{\mathcal{H}}_{2:3}}{\partial K} \frac{1}{\partial \tilde{\mathcal{H}}_{2:3}/\partial p} T_K d\sigma \tag{58}$$

Then, the methodology using the pendulum model approximation is adapted. Subtracting the value of the Hamiltonian evaluated at the saddle point, the new Hamiltonian $\bar{\mathcal{H}}_{2:3}$ is

$$\bar{\mathcal{H}}_{2:3} = -\frac{1}{2}\alpha p^2 + 2\hat{A}\sin^2\frac{\sigma}{2} \tag{59}$$

By performing the change of variable $s = \sigma/2$, The Hamiltonian reduces to

$$\bar{\mathcal{H}}_{2:3} = -\frac{1}{2}\alpha p^2 + 2\hat{A}\sin^2(s) \tag{60}$$

and the formulation of the probability of capture in Eq. 56 is used.

4 Results

In the following section, the estimation methodologies are referred to as follows: the numerical methodology uses Eq. 43, the semi-analytical methodology uses Eq. 44, and the analytical methodology uses Eq. 56.

4.1 Simulation setup

To estimate numerically the probability of capture, 1000 different trajectories are propagated inside the interval of initial conditions defined in the tables at the beginning of Sections 4.2 (Table 1) and 4.3 (Table 2). The initial conditions are uniformly distributed: 100 different initial semi-major axis values and 10 different resonance angle values. The equation of motion are propagated for 20 days using the MATLAB built-in function `ode113` which is a variable-step, variable-order Adams-Bashforth-Moulton solver of orders 1 to 13 [27], with a relative and absolute tolerance set at 10^{-12}.

The mean probability of capture values, later introduced in Sections 4.2 and 4.3, are calculated taking the average of 1000 different thrust magnitude values for 1000 different initial conditions.

4.2 1:1 GTR

This section presents the estimations obtained using the semi-analytical and analytical methods and compares them with the numerical estimations. The probability of capture is estimated for three cases based on the thrust magnitude intervals: high thrust magnitude cases with $T = [20, 90]$ mN, low thrust magnitude cases with $T = [0.2, 20]$ mN, and very low-thrust magnitude cases with $T = [0.02, 0.2]$ mN. If not specified, the initial conditions for the simulations are listed in Table 1.

Table 1: Initial conditions.

Resonance angle	$[0, 2\pi]$
Semi-major axis	[690,700] km
eccentricity	0.5

4.2.1 Sensitivity on the thrust magnitude

The probability estimations obtained using the three approaches are compared and presented in Fig. 5. The probability estimated numerically is represented with a black line in the three plots, while the semi-analytical and analytical results are represented by red and blue lines, respectively. The semi-analytical and analytical estimations of probability are found to be independent of the thrust magnitude. For the very low-thrust magnitude cases, the semi-analytical estimation is in good agreement with the average numerical estimation, while the analytical one overestimates the probability. As the thrust magnitude increases, the probability of capture decreases on average and the semi-analytical and analytical methodologies do not follow this trend. For the high thrust magnitude case, the numerically estimated probability of capture shows an oscillatory behavior, and the analytical/semi-analytical estimation methodologies are not able to accurately estimate the probability of capture. For this reason, in the last part of the paper, the thrust magnitude interval between 0.02 mN and 0.2 mN is considered.

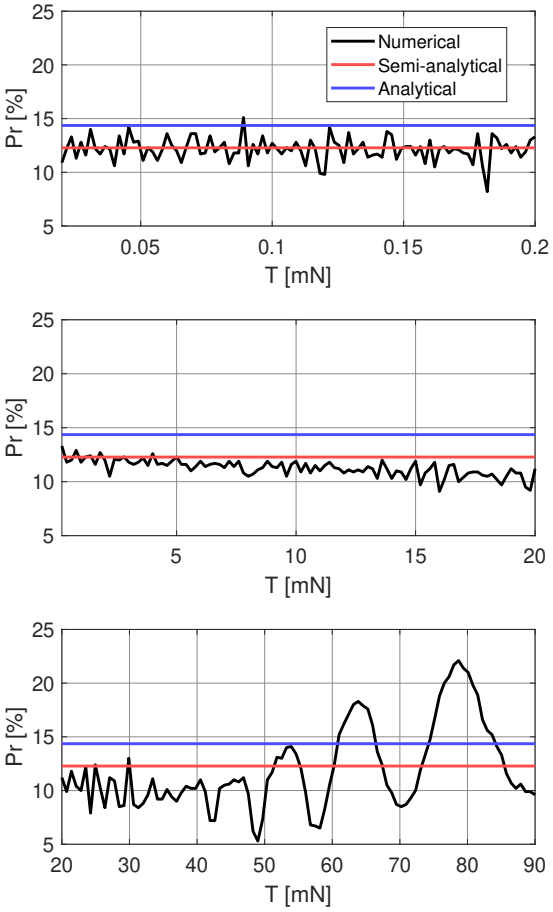

Figure 5: Probability of capture into 1:1 GTR evolution for $e = 0.5$ and for different thrust magnitude values estimated with numerical (in black), semi-analytical (in red) and analytical (in blue) methodologies. Very low-thrust, low-thrust and high-thrust cases are shown in the upper, middle and lower plots, respectively.

4.2.2 Sensitivity on the initial eccentricity

This section examines the sensitivity of the probability of capture to variations in initial eccentricity. In accordance with the setup delineated in Section 4, the probability of capture into a 1:1 GTR is estimated across a range of eccentricity values. Figure 6 illustrates the mean probability of capture for eccentricities ranging from 0 to 0.6. The analytically estimated mean probability of capture remains constant across all values of eccentricity. For low eccentricities, the probabilities estimated by the semi-analytical

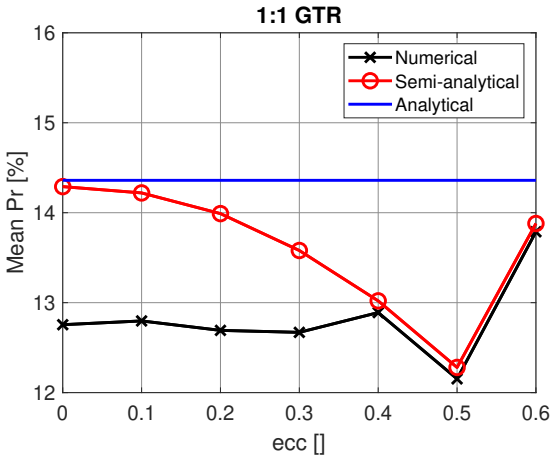

Figure 6: Mean probability of capture into 1:1 GTR evolution for very low-thrust magnitude values and for different eccentricity values estimated with numerical (in black), semi-analytical (in red) and analytical (in blue) methodologies.

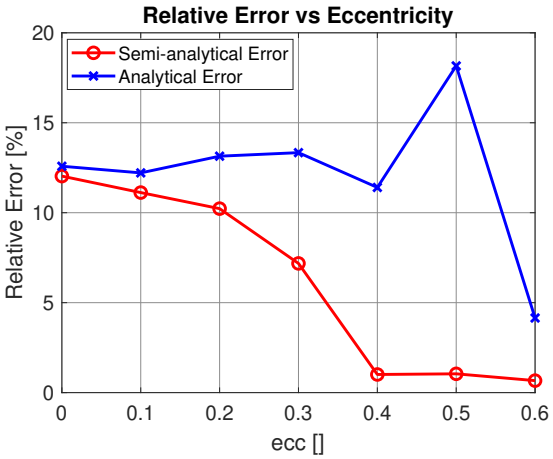

Figure 7: Relative error between the estimations of the probability of capture into 1:1 GTR for different eccentricity values using the semi-analytical (in red) and analytical (in blue) methodologies with respect to the numerical estimations.

and analytical methods are in agreement. However, as the eccentricity increases, the semi-analytical estimation tends to converge with the numerical estimation.

In particular, for low values of eccentricity, the numerical estimation remains relatively constant at approximately 12.7%, whereas it rises to around 13.8% with increasing eccentricity. The analytical estimation, represented by the blue line, consistently provides a value close to 14.4%, thereby serving as an upper bound for the mean probability of capture. For high-eccentricity scenarios $e > 0.4$, the semi-analytical estimation provides an accurate measure of the probability of capture. Figure 7 displays the relative errors of the semi-analytical and analytical methods in comparison to the numerical estimation. The relative error Err_{rel} between the analytical and numerical estimates is calculated as

$$Err_{\text{rel}} = \left| \frac{Pr_{\text{an}} - Pr_{\text{num}}}{Pr_{\text{num}}} \right| \times 100 \tag{61}$$

Here, Pr_{an} and Pr_{num} represent the probabilities of capture estimated analytically and numerically, respectively. In a similar way, the relative error between semi-analytical and numerical is defined. In the semi-analytical case, the error reaches a peak value of approximately 12% for $e = 0$ (representing the worst-case scenario), whereas the error does not exceed 1% for high-eccentricity cases. For the analytical method, the relative error reaches a maximum value of approximately 18.1%, converging to the numerical estimate only in the case of extreme eccentricity $e = 0.6$.

4.3 2:3 GTR

In this section, the probability of capture into 2:3 GTR estimations obtained through semi-analytical and analytical methodologies are outlined and compared with numerical estimations. Focus is placed solely on cases involving very low-thrust magnitudes, as done for the 1:1 GTR. Unless otherwise indicated, the initial conditions for these simulations are provided in Table 2.

Table 2: Initial conditions.

Resonance angle	$[0, 2\pi]$
Semi-major axis	[990,1000] km
eccentricity	[0 0.55]

4.3.1 Sensitivity on the initial eccentricity

This section investigates the sensitivity of the probability of capture into 2:3 GTR with respect to variations in initial eccentricity. Consistent with the framework outlined in Section 4, probabilities of capture for a range of eccentricity values are estimated. Figure 8 shows the mean probability of capture for eccentricities between 0 and 0.55. This discussion begins by focusing on the numerical results. Unlike the 1:1 GTR case, the distribution of solutions shows a different trend. For high-eccentricity cases, the estimated probability of capture is around 16.6%. As

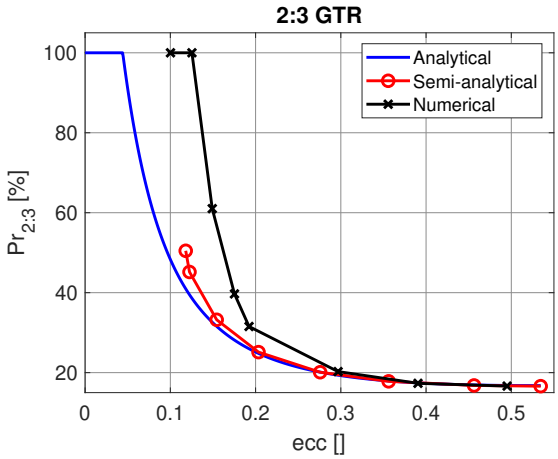

Figure 8: Mean probability of capture into 2:3 GTR evolution for very low-thrust magnitude values and for different eccentricity values estimated with numerical (in black), semi-analytical (in red) and analytical (in blue) methodologies.

eccentricity decreases, the probability value increases exponentially, reaching a value of 100% when $e = 0.13$. For $e < 0.13$, the probability is estimated to be 100%. It is noteworthy that numerical estimations stop for $e < 0.1$ due to the difficulty of defining the separatrices at lower eccentricities as shown in Fig. 9. The resonance region continues to decrease in size, until it collapses for $e = 0$. This is also the case for the semi-analytical results. When the probability of capture is 100%, the phenomenon of "automatic entry into libration" occurs [28]. Neishtadt [25] discussed and motivated this mechanism for Saturn's satellite system, identifying the cause in the Hamiltonian's singularity ($e = 0$). The same singularity is present in this case which brings about the "automatic entry into libration" phenomenon.

Overall, both semi-analytical and analytical methodologies align closely with the numerical results for high eccentricity cases. Figure 10 shows the relative errors, defined in Eq. 61, of these two methodologies in comparison to the numerical estimations. For $e > 0.3$, the relative errors of both methodologies remain below 5%. As eccentricity decreases, the relative errors for the two methodologies remain close, reaching values of 61% and 55% for the analytical and semi-analytical approaches, respectively. This shows that for low-eccentricity cases a different approach is needed.

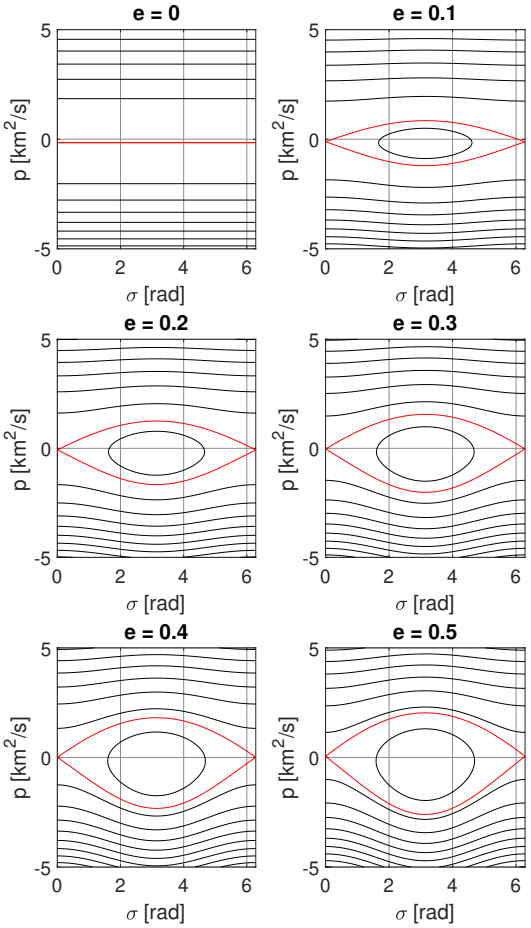

Figure 9: Phase space of the 2:3 GTR evolution for different eccentricity values. The red lines represent the separatrix lines.

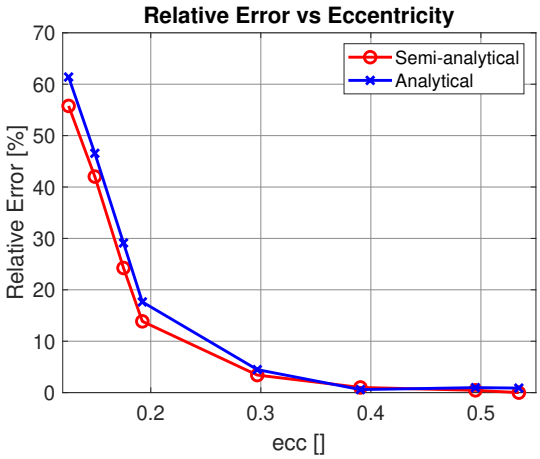

Figure 10: Relative error between the estimations of the probability of capture into 2:3 GTR for different eccentricity values using the semi-analytical (in red) and analytical (in blue) methodologies with respect to the numerical estimations.

5 Advantages of Analytical and Semi-Analytical Methodologies

In this section, the unique advantages of employing analytical and semi-analytical methodologies over numerical methods are discussed.

5.1 In-depth Understanding of Dynamical Systems

Utilizing semi-analytical and analytical approaches facilitates a comprehensive examination of the dynamical phenomena involved in the estimation of the probability of capture into GTRs. Beyond characterizing resonance regions, such as their location and width, these methodologies enable a deeper understanding of previously unexplored phenomena. Notably, the ”automatic entry into libration” phenomenon, discussed by Sinclair [28] and Neishtadt [25], is introduced into the field of astrodynamics for the first time through these methods.

5.2 Computational Efficiency

The analytical and semi-analytical approaches offer remarkable computational efficiency compared to numerical methods. In the preceding section, the mean probability of capture was estimated for each value of eccentricity using 1000 different initial conditions across 100 different thrust magnitudes, uniformly distributed in the interval $T = [0.02, 0.2]$ mN. This amounts to a total of 100,000 separate cases for each eccentricity value. The computational time required for each eccentricity value averaged to approximately four days using numerical methods. The new methodologies dramatically reduce this time requirement: the semi-analytical approach requires on the order of minutes, while the analytical method necessitates only seconds to estimate the probabilities across all eccentricity values.

6 Conclusion

This study has focused on the development and validation of analytical and semi-analytical methodologies for estimating the probability of capture into GTRs. The mathematical models of each GTR are formulated and the methodologies are developed from the energy balance of the system as it crosses the resonance region. A comparative study was performed against traditional numerical methods, and our models were validated using a wide range of eccentricity and thrust magnitude values. The methodologies proved themselves to estimate accurately the probability of capture into GTRs for high eccentricity cases and for very low-thrust magnitudes. The semi-analytical methodology was found to be characterized by a smaller error compared to the analytical methodology for both 1:1 and 2:3 GTR. Generally, the advantages of these methodologies over traditional numerical approaches are twofold. Firstly, they provide an in-depth understanding of the dynamical systems involved in GTRs. This enables better characterization of resonance regions and introduces the phenomenon of ”automatic entry into libration” into astrodynamics. Secondly, the computational efficiency offered by these methodologies is noteworthy. With an average computational time of just minutes for semi-analytical methods and seconds for analytical ones, these methodologies stand as powerful tools for real-time applications and for studies that require extensive uncertainty quantification analysis.

While these methods prove to be effective and efficient for the conditions tested, it is acknowledged that they may not guarantee the correct estimation, especially for low-eccentricity cases. Future work should focus on extending these methodologies to this range of eccentricity. This work distinguishes itself by venturing into previously unexplored areas of dynamical phenomena, most notably the ”automatic entry into libration” phenomenon, thereby contributing significantly to the field of astrody-

namics. The contributions of this study lay the path for future research aimed at increasing our understanding and capabilities in astrodynamics.

Acknowledgements

This work is funded by ESA OSIP with project title "Resonance Capture of Low-Thrust Spacecraft Around a Small Body" and by the John Anderson Research Award Studentship.

References

[1] A. Artemyev, A. Neishtadt, D. Vainchtein, A. Vasiliev, I. Vasko, and L. Zelenyi, "Trapping (capture) into resonance and scattering on resonance: Summary of results for space plasma systems," *Communications in Nonlinear Science and Numerical Simulation*, vol. 65, pp. 111–160, 2018.

[2] B. Garfinkel, "On resonance in celestial mechanics," *Celestial Mechanics*, vol. 28, pp. 275–290, 1982.

[3] P. Tricarico and M. Sykes, "The dynamical environment of Dawn at Vesta," *Planetary and Space Science*, vol. 58, pp. 1516–1525, 2010.

[4] C. D. Murray and S. F. Dermott, "Solar System Dynamics," *Cambridge University Press*, 2000.

[5] A. Celletti, C. Gales, and C. Lhotka, "(INVITED) Resonances in the Earth's space environment," *Communications in Nonlinear Science and Numerical Simulation*, vol. 84, pp. 105–185, 2020.

[6] A. Lemaître, N. Delsate, and S. Valk, "A web of secondary resonances for large A/m geostationary debris," *Celestial Mechanics and Dynamical Astronomy*, vol. 104, pp. 383–402, 2009.

[7] P. Goldreich and S. Peale, "Spin–orbit coupling in the Solar System," *Astronomical Journal*, vol. 71, pp. 425–438, 1966.

[8] A. Celletti and C. Gales, "On the Dynamics of Space Debris: 1:1 and 2:1 Resonances," *Journal of Nonlinear Science*, vol. 24, pp. 1231–1262, 2014.

[9] D. Scheeres, "Dynamics about uniformly rotating triaxial ellipsoids: Applications to asteroids," *Icarus*, vol. 110, pp. 225—238, 1994.

[10] D. Scheeres, S. Ostro, R. Hudson, E. DeJong, and S. Suzuki, "Dynamics of Orbits Close to Asteroid 4179 Toutatis," *Icarus*, vol. 132, pp. 53–79, 1998.

[11] D. Scheeres, M. D. Guman, and B. F. Villac, "Stability Analysis of Planetary Satellite Orbiters: Application to the Europa Orbiter," *Journal of Guidance, Control, and Dynamics*, vol. 24, 2001.

[12] M. E. Paskowitz and D. Scheeres, "Design of Science Orbits About Planetary Satellites: Application to Europa," *Journal of Guidance, Control, and Dynamics*, vol. 29, 2006.

[13] R. Russell, "Global search for planar and three-dimensional periodic orbits near Europa," *The Journal of the Astronautical Sciences*, vol. 54, pp. 199–226, 2006.

[14] M. Lara and R. Russell, "Mission design through averaging of perturbed Keplerian systems: the paradigm of an Enceladus orbiter," *Celestial Mechanics and Dynamical Astronomy*, vol. 108, pp. 1–22, 2010.

[15] R. Russell and M. Lara, "On the design of an Enceladus science orbit," *Acta Astronautica*, vol. 65, pp. 27–39, 2009.

[16] K. Nishiyama, S. Hosoda, K. Ueno, R. Tsukizaki, and H. Kuninaka, "Development and Testing of the Hayabusa 2 Ion Engine System," *The Japan Society for Aeronautical and Space Sciences*, vol. 14, pp. 131–140, 2016.

[17] N. Wallace, O. Sutherland, J. Bolter, H. Gray, A. Altay, F. Striedter, F. Budnik, S. Manganelli, E. Montagnon, and C. Steiger, "BepiColombo - Solar Electric Propulsion System Operations for the transit to Mercury," *36th International Electric Propulsion Conference, Vienna*, 2019.

[18] D. Morante, M. Sanjurjo Rivo, and M. Soler, "A Survey on Low-Thrust Trajectory Optimization Approaches," *Aerospace*, vol. 88, 2021.

[19] D. Scheeres, "Orbital mechanics about small bodies," *Acta Astronautica*, vol. 72, pp. 1–14, 2012.

[20] W. Kaula, "Theory of Satellite Geodesy: Applications of Satellites to Geodesy," *Blaisdell Publishing Co.*, 1966.

[21] D. Scheeres, "The effect of C_{22} on orbit energy and angular momentum," *Celestial Mechanics and Dynamical Astronomy*, vol. 73, pp. 339—-348, 1999.

[22] C. Lhotka, A. Celletti, and C. Gales, "Poynting–Robertson drag and solar wind in the space debris problem," *Monthly Notices of the Royal Astronomical Society*, vol. 460, pp. 802–815, 2016.

[23] D. Okhotsimskii and Y. Sikharulidze, *Fundamentals of Space Flight Mechanics*, 1990.

[24] A. Neishtadt, "Averaging method for systems with separatrix crossing," *Nonlinearity*, vol. 30, 2017.

[25] ——, "Passage through a separatrix in a resonance problem with a slowly-varying parameter," *Journal of Applied Mathematics and Mechanics*, vol. 4, 1975.

[26] L. F. Shampine, "Vectorized adaptive quadrature in matlab," *Journal of Computational and Applied Mathematics*, vol. 211, pp. 131–140, 2008.

[27] L. F. Shampine and M. K. Gordon, *Computer Solution of Ordinary Differential Equations: the Initial Value Problem*. San Francisco: W. H. Freeman, 1975.

[28] A. T. Sinclair, "On the Origin of the Commensurabilities Amongst the Satellites of Saturn," *Monthly Notices of the Royal Astronomical Society*, vol. 160, 1972.